Catalysis Today 164 (2011) 308–314

Contents lists available at ScienceDirect

Catalysis Today

journal homepage: www.elsevier.com/locate/cattod

Synthesis of ethanol from syngas over $Rh/Ce_{1-x}Zr_xO_2$ catalysts

Yanyong Liu*, Kazuhisa Murata, Megumu Inaba, Isao Takahara, Kiyomi Okabe

Energy Technology Research Institute, National Institute of Advanced Industrial Science and Technology, AIST Tsukuba Central 5, Higashi 1-1-1, Tsukuba 305-8565, Japan

ARTICLE INFO

Article history:
Received 30 June 2010
Received in revised form 25 October 2010
Accepted 26 October 2010
Available online 3 December 2010

Keywords:
Ethanol synthesis
Syngas
Rh catalyst
$Ce_{1-x}Zr_xO_2$ support
Reducibility
Acidity–basicity

ABSTRACT

$Rh/Ce_{1-x}Zr_xO_2$ (x = 0–1) samples (with 2 wt% Rh loading) were prepared by a coprecipitation method using $NH_3{\cdot}H_2O$ as a precipitant. The resultant samples were used as catalysts for the synthesis of ethanol from syngas in a high-pressure fixed-bed flow reactor under typical reaction conditions of T = 548 K, P = 2.4 MPa, H_2/CO = 2/1, and W/F = 10 g h mol^{-1}. XRD results indicated that Zr^{4+} ions entered in the CeO_2 lattices when x was less than 0.2 in $Rh/Ce_{1-x}Zr_xO_2$. TPR results indicated that the reducibility of CeO_2 increased by inducing Zr^{4+} ions into the CeO_2 lattices in $Rh/Ce_{0.8}Zr_{0.2}O_2$. NH_3-TPD and CO_2-TPD results indicated that $Rh/Ce_{0.8}Zr_{0.2}O_2$ contained both acid sites and base sites on the surface. Rh/CeO_2 showed a CO conversion of 23.7%, which was higher than those over Rh/SiO_2 (10.1%), Rh/MgO (10.8%), and Rh/ZrO_2 (18.2%) at 548 K because a strong interaction between support and metal (SISM) existed in Rh/CeO_2. Moreover, the CO conversion over $Rh/Ce_{0.8}Zr_{0.2}O_2$ (27.3%) was higher than that over Rh/CeO_2 (23.7%) due to the smaller Rh particle size and the stronger reducibility in $Rh/Ce_{0.8}Zr_{0.2}O_2$. The main oxygenated products were acetaldehyde and ethanol over neutral or acidic supports supported Rh catalysts (Rh/SiO_2, Rh/ZrO_2), and were methanol and ethanol over basic supports supported Rh catalysts (Rh/MgO, Rh/CeO_2, $Rh/Ce_{0.8}Zr_{0.2}O_2$). $Rh/Ce_{0.8}Zr_{0.2}O_2$ showed the highest selectivity for ethanol among various catalysts because the $Ce_{0.8}Zr_{0.2}O_2$ support simultaneously possesses reducibility, acidity and basicity.

© 2010 Elsevier B.V. All rights reserved.

1. Introduction

The use of biomass feedstocks (such as agriculture and forestry residues) for generating energy has become increasingly important in recent years because of the global climate change and the depletion of fossil fuel resources. Ethanol has attracted great attention because it can be used as a fuel additive and as a hydrogen carrier. Ethanol can be produced from biomass using a biological fermentation process (through a sugar platform) and using a chemical BTL (biomass to liquid) process (through a syngas platform) [1,2]. The fermentation process is limited in its application only to selected biomass components for ethanol production because the lignin component in the woody biomass cannot be converted by the current fermentation process. In contrast, all kinds of biomass resource can be converted by the BTL process, because syngas can be obtained from all biomass feedstocks by gasification and/or reforming.

Four kinds of catalysts have been used in the synthesis of higher alcohols from syngas: Rh-based [3–5], Mo-based [6], modified F–T synthesis [7], and modified methanol synthesis catalysts [8,9]. Rh-based catalysts showed the best selectivity for ethanol among various catalysts [1,2]. However, because Rh metal is very expensive, the improvement of the activity and the selectivity for ethanol over Rh-based catalysts is necessary for achieving a commercial available process. The support and the promoter are important to develop highly active Rh-based catalysts for the synthesis of ethanol from syngas [3–5]. Rare earth oxides have been reported as efficient promoters for Rh/SiO_2 catalysts in the synthesis of ethanol [10–13]. A strong interaction between support and metal (SISM) exists in the CeO_2-supported metal catalysts and gives the catalysts high activity for many reactions [14–17]. Introduction of Zr^{4+} ions into the CeO_2 lattices improves the catalytic performance of CeO_2-supported metal catalysts for some reactions through changing the physical and chemical property of the supports [18–22]. In the present study, we investigated the catalytic performance of $Rh/Ce_{1-x}Zr_xO_2$ catalysts for the synthesis of ethanol from syngas.

2. Experimental

2.1. Catalyst preparation

$Rh/Ce_{1-x}Zr_xO_2$ (x = 0–1) was prepared by a coprecipitation method using $NH_3{\cdot}H_2O$ as a precipitant in order to avoid the residues of alkali metals [9]. In a typical process, a solution of 28 wt% $NH_3{\cdot}H_2O$ was added to an aqueous solution of mixed metallic nitrates of $Ce(NO_3)_3$, $ZrO(NO_3)_2$, and $Rh(NO_3)_3$ till pH = 10 at room temperature with strong stirring. Then, the slurry was aged at 363 K for 1 h. A precipitate was obtained after filtering the slurry

* Corresponding author. Fax: +81 0298 61 4776.
E-mail address: yy.ryuu@aist.go.jp (Y. Liu).

0920-5861/$ – see front matter © 2010 Elsevier B.V. All rights reserved.
doi:10.1016/j.cattod.2010.10.087

at room temperature. The resultant precipitate was then dried at 373 K for 24 h, and finally calcined at 723 K for 3 h. The Rh loading was 2 wt% in the sample.

Rh/MgO was prepared using a method similar to that for preparing $Rh/Ce_{1-x}Zr_xO_2$. The $NH_3{\cdot}H_2O$ precipitant was added to a mixed aqueous solution of $Mg(NO_3)_2$ and $Rh(NO_3)_3$ till pH = 10 at room temperature with strong stirring. The slurry was aged at 363 K for 1 h and a precipitate was obtained after filtration. The resultant precipitate was dried at 373 K for 24 h and calcined at 723 K for 3 h. The Rh loading was 2 wt% in the sample.

The Rh/SiO_2 catalyst was prepared by the impregnation of SiO_2 (JRC-SIO-1, 300 $m^2\,g^{-1}$) with an aqueous solution of $Rh(NO_3)_3$. The sample was then dried at 373 K for 24 h, and finally calcined at 723 K for 3 h. The Rh loading was 2 wt% in the sample.

2.2. Catalyst characterization

X-ray powder diffraction (XRD) patterns were measured using a MAC Science MXP-18 diffractometer with a Cu-Kα radiation at 40 kV and 50 mA. Inductively coupled plasma (ICP) analyses were measured by a Thermo Jarrel Ash IRIS/AP instrument. Temperature programmed reduction (TPR) was carried out in a U-shaped quartz tube (i.d. = 3 mm, l = 150 mm) with a mixture of 10% H_2 and 90% Ar. The gas flow rate was 30 ml min^{-1} and the sample was heated from 298 to 973 K (heating rate: 5 K min^{-1}). BET surface areas were measured by N_2 adsorption at 77 K and the particle sizes of supported Rh were measured by a CO pulse method at room temperature using a BELCAT-B automatic instrument. In the measurement of Rh particle size, a catalyst of 20 mg was reduced in 100 ml min^{-1} of H_2 at 673 K for 20 min and then cooled down. The CO pulse measurement was carried out at room temperature. The CO uptake was estimated by the extrapolation to zero pressure of the linear part of the isotherms. The difference between the total amount of adsorbed CO (CO_{tot}) and the reversible part of adsorbed CO (CO_{rev}) gave the irreversible part of adsorbed CO (CO_{irr}). The amount of CO_{irr} was used for calculating the Rh particle size (assuming stoichiometry: $CO_{irr}/Rh = 1$). NH_3-TPD and CO_2-TPD were measured using an atmospheric flow system (BELCAT-B) with a TCD and a Q-mass (QMG220 PrismaPlus). The sample (0.05 g) was pretreated at 673 K for 1 h under a He flow (50 ml min^{-1}). After the temperature decreased to 323 K, NH_3 or CO_2 was introduced for adsorbing on the surface, followed by evacuation at 323 K for 1 h to eliminate the weakly physical adsorbed species. Then, NH_3-TPD or CO_2-TPD was carried out from 323 K to 973 K (heating rate: 5 K min^{-1}). The recorded TCD signal was checked by the Q-mass at m/e = 17 (for NH_3), 44 (for CO_2), and 18 (for H_2O) during the TPD measurement.

2.3. Catalyst measurement

The catalytic reaction was carried out in a high-pressure fixed-bed flow reaction system at 473–573 K under a total pressure of 2.4 MPa. After 1.0 g catalyst and 2.0 g quartz sand were mixed uniformly, they were packed in a tubular reactor (i.d. = 10 mm). Prior to the reaction, the catalyst was reduced in a H_2 flow (50 ml min^{-1}) at 573 K for 1 h. The feed gas contained 60% H_2, 30% CO and 10% N_2 (using as an internal standard). The products were analyzed by three on-line GCs during the reaction. H_2, N_2, CO, and CO_2 were analyzed by a TCD and a New Carbon-ST column; light hydrocarbons (C_1–C_4) were analyzed by a FID and a CP-Al_2O_3/KCl capillary column; heavy hydrocarbons (C_{5+}) were analyzed by a FID and a UA-DX capillary column; and oxygenated compounds were analyzed by a FID and a Stablewax capillary column. CO conversion was determined by the changes of the percentage concentrations of CO and N_2 (internal standard) in the mixed gases before and after the reaction. Product selectivities were reported in terms of carbon efficiencies which were calculated by using the formula $n_iC_i/\Sigma(n_iC_i)$ where n_i is the carbon atom number of the compound.

3. Results and discussion

3.1. Characterization of $Rh/Ce_{1-x}Zr_xO_2$ samples

Fig. 1 shows the XRD pattern of various $Rh/Ce_{1-x}Zr_xO_2$ samples with 2 wt% Rh loading after calcination at 723 K for 3 h. The reflections of Rh_2O_3 phase could not be observed in the XRD pattern of each sample, implying the high dispersion of Rh_2O_3 particles in the samples. Rh/CeO_2 showed four strong reflections corresponding to (1 1 1), (2 0 0), (2 2 0) and (3 1 1) crystallographic planes of CeO_2 support, indicating that the CeO_2 support had a fluorite structure with cubic (f c c) cells. Although Rh/ZrO_2 also showed four strong reflections corresponding to cubic ZrO_2 cells in the XRD pattern, the position of each reflection in Rh/ZrO_2 was obviously different from that of Rh/CeO_2 due to the different ionic radius of Zr^{4+} and Ce^{4+} ions (Zr^{4+}: 0.79 nm; Ce^{4+}: 0.92 nm [23]). In the XRD pattern of $Rh/Ce_{0.8}Zr_{0.2}O_2$, the reflections of CeO_2 phase were very strong but the reflections of ZrO_2 phase could not be observed. This implies that Zr^{4+} ions entered in the CeO_2 lattices to form a homogeneous solid solution in $Rh/Ce_{0.8}Zr_{0.2}O_2$. On the other hand, Ce^{4+} ions entered in the ZrO_2 lattices in $Rh/Ce_{0.2}Zr_{0.8}O_2$ from the results of the XRD pattern. In the XRD pattern of $Rh/Ce_{0.5}Zr_{0.5}O_2$, the reflections were very weak although the pattern of CeO_2 could be observed, implying the collapse of CeO_2 cells in $Rh/Ce_{0.5}Zr_{0.5}O_2$.

Fig. 2 shows the BET surface area and Rh particle size in $Rh/Ce_{1-x}Zr_xO_2$ with 2 wt% Rh loading after reduction at 573 K for 1 h. The doping of Zr^{4+} ions decreased the crystallization degree of CeO_2 (Fig. 1), which caused an increase in the BET surface area when x was less than 0.2 in $Rh/Ce_{1-x}Zr_xO_2$ [9,18]. When x was larger than 0.2 in $Rh/Ce_{1-x}Zr_xO_2$, some Zr^{4+} ions could not enter in the CeO_2 lattices and they formed ZrO_2 particles on the catalyst surface, which caused a decrease in the BET surface area [9,18]. The Rh particle size was calculated from the actual loading of Rh metal and the amount of adsorbed CO molecules for each catalyst. The actual Rh loadings,

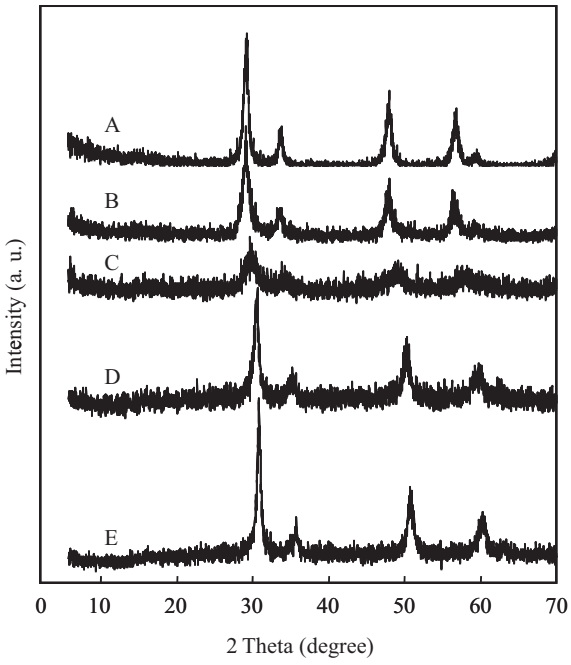

Fig. 1. XRD patterns of various $Rh/Ce_{1-x}Zr_xO_2$ samples with 2 wt% Rh loading after calcination at 723 K for 3 h. (A) Rh/CeO_2; (B) $Rh/Ce_{0.8}Zr_{0.2}O_2$; (C) $Rh/Ce_{0.5}Zr_{0.5}O_2$; (D) $Rh/Ce_{0.2}Zr_{0.8}O_2$; and (E) Rh/ZrO_2.

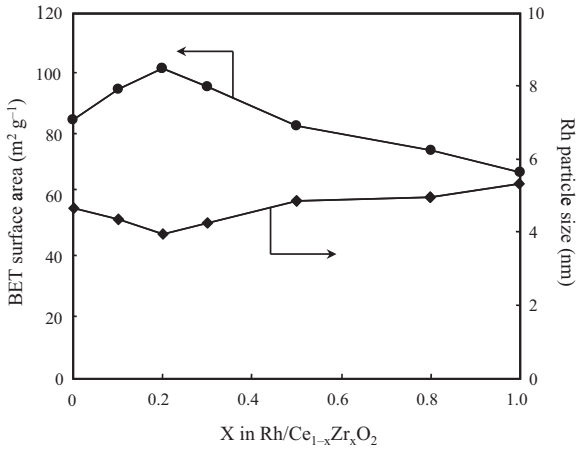

Fig. 2. BET surface area and Rh particle size in $Rh/Ce_{1-x}Zr_xO_2$ with 2 wt% Rh loading after reduction at 573 K for 1 h. (●) BET surface area; (■) Rh particle size.

which were measured by ICP analysis, were similar to the designed Rh loadings for various catalysts. The Rh particle size decreased with increasing Zr amount at $x < 0.2$ but increased with increasing Zr amount at $x > 0.2$ in $Rh/Ce_{1-x}Zr_xO_2$. $Rh/Ce_{0.8}Zr_{0.2}O_2$ showed the smallest Rh particle size among $Rh/Ce_{1-x}Zr_xO_2$ owing to the largest BET surface area and the strongest SISM effect [9,18]. The Rh particle size in 2 wt% $Rh/Ce_{0.8}Zr_{0.2}O_2$ was about 4 nm, which is a suitable size for the synthesis of ethanol from syngas over Rh-based catalysts [12,24].

Fig. 3 shows the TPR profiles of various $Rh/Ce_{1-x}Zr_xO_2$ samples with 2 wt% Rh loading after calcination at 723 K for 3 h. The peak at 393 K could be observed in the TPR profile of each sample due to the reduction of Rh^{3+} ($Rh^{3+} \rightarrow Rh^0$). Rh/ZrO_2 did not show a reduction peak of ZrO_2 support below 973 K. Rh/CeO_2 showed a reduction peak at about 853 K owing to the partial reduction of the CeO_2 support ($Ce^{4+} \rightarrow Ce^{3+}$). As for $Rh/Ce_{0.8}Zr_{0.2}O_2$, it showed three reduction peaks in the TPR profile: the peak at 393 K owing to the reduction of Rh^{3+}, the peak at 483 K owing to the partial reduction of surface Ce^{4+}, and the peak at 703 K owing to the partial reduction of Ce^{4+} in the bulk [25–27]. $Rh/Ce_{0.5}Zr_{0.5}O_2$ and $Rh/Ce_{0.2}Zr_{0.8}O_2$ also showed the peaks owing to the partial reduction of surface Ce^{4+} and bulk Ce^{4+} in the TPR profiles. The isovalent substitution by Zr^{4+} ions in the lattices of CeO_2 created defects on the surface and in the bulk. The defects throughout the crystal produced an increase

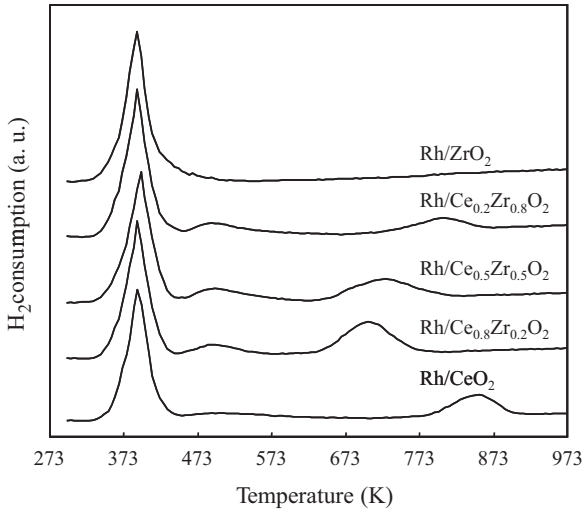

Fig. 3. TPR profiles of various $Rh/Ce_{1-x}Zr_xO_2$ samples with 2 wt% Rh loading after calcination at 723 K for 3 h.

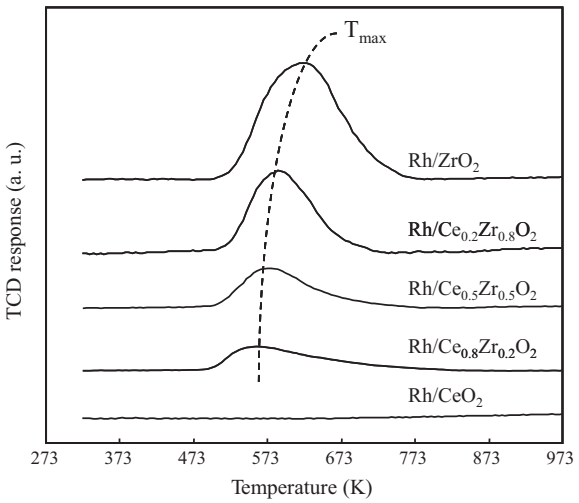

Fig. 4. NH_3-TPD profiles of various $Rh/Ce_{1-x}Zr_xO_2$ samples with 2 wt% Rh loading after calcination at 723 K for 3 h.

in the oxygen mobility and diffusion in the lattices, which promoted the reduction of Ce^{4+} in the $Ce_{0.8}Zr_{0.2}O_2$ solid solution [28]. Moreover, the addition of noble metals to the CeO_2-based materials strongly enhanced the reducibility of the Ce^{4+} due to the hydrogen spillover on the surface [29]. The surface oxygen vacancies were introduced by hydrogen spillover from the noble metal to the solid solution, and then these vacancies at the surface were subsequently filled up by the bulk oxygen being transported to the surface due to the ionic conductivity [30]. Furthermore, the strong interaction between support and metal (SISM) influences the reducibility of $Ce_{1-x}Zr_xO_2$-supported metal catalysts [14–17]. The partial reduction of surface Ce^{4+} ions at 483 K in Fig. 3 may be caused by the SISM effect between Rh and $Ce_{1-x}Zr_xO_2$ support. It have been reported that $Rh/Ce_{1-x}Zr_xO_2$ samples which calcined at 953 K even showed a split in the reduction peak of Rh_2O_3 [31]. The split was also caused by the SISM effect in the $Rh/Ce_{1-x}Zr_xO_2$ samples [31]. On the other hand, the samples in this study (calcined at 723 K) showed very similar patterns at above 473 K to the samples in literature (calcined at 953 K) [31].

Fig. 4 shows the NH_3-TPD profiles of various $Rh/Ce_{1-x}Zr_xO_2$ samples with 2 wt% Rh loading after calcination at 723 K for 3 h. NH_3-TPD is usually used for evaluating the acid strength and the acid amount in the solid acids. The acid strength was characterized by the desorbed temperature of NH_3 molecules and the acid amount was characterized by the total number of desorbed NH_3 molecules on the solid surface. The NH_3 molecules physically adsorbed on the samples were eliminated before TPD measurement by evacuation treatment at 323 K. As shown in Fig. 4, Rh/CeO_2 did not show a peak in the NH_3-TPD profile, indicating that there is not acid site on the Rh/CeO_2 surface. $Ce_{0.8}Zr_{0.2}O_2$ showed a NH_3 desorbed peak at $T_{max} = 563$ K in the NH_3-TPD profile, implying that introducing Zr^{4+} ions into Rh/CeO_2 brought acidic sites to the catalyst surface [18–20]. ZrO_2 is an acidic support because Rh/ZrO_2 showed a large peak at $T_{max} = 593$ K in the NH_3-TPD profile. Both the peak area and the maximum desorbed temperature increased with increasing Zr amount in $Rh/Ce_{1-x}Zr_xO_2$, indicating that both the acid amount and the acid strength increased with increasing Zr amount in $Rh/Ce_{1-x}Zr_xO_2$.

Fig. 5 shows the CO_2-TPD profiles of various $Rh/Ce_{1-x}Zr_xO_2$ samples with 2 wt% Rh loading after calcination at 723 K for 3 h. CO_2-TPD is usually used for evaluating the base strength and the base amount in the solid bases. The CO_2 molecules physically adsorbed on the samples were eliminated before TPD measurement by evacuation treatment at 323 K. For convenience, the base sites

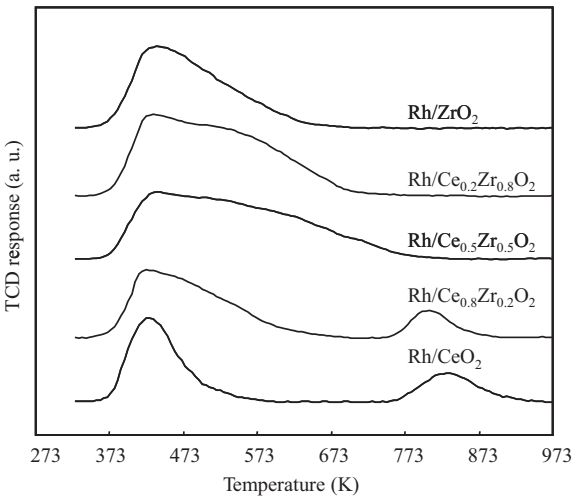

Fig. 5. CO_2-TPD profiles of various $Rh/Ce_{1-x}Zr_xO_2$ samples with 2 wt% Rh loading after calcination at 723 K for 3 h.

from which CO_2 molecules were desorbed at temperatures lower than 523 K were designated as weak base sites; those from which CO_2 molecules were desorbed from 523 K to 723 K, medium base sites; and those from which CO_2 molecules were desorbed at temperatures greater than 723 K, strong base sites. As shown in Fig. 5, Rh/ZrO_2 showed the only peak at T_{max} = 423 K in the CO_2-TPD profile, implying that Rh/ZrO_2 possessed only weak base sites on the surface. Rh/CeO_2 showed a peak at low temperature (T_{max} = 423 K) and a peak at high temperature (T_{max} = 823 K) in the CO_2-TPD profile, indicating that Rh/CeO_2 contained both weak base sites and strong base sites on the surface. $Rh/Ce_{0.8}Zr_{0.2}O_2$ showed a peak at T_{max} = 793 K corresponding to strong base sites but $Rh/Ce_{0.5}Zr_{0.5}O_2$ did not show a peak of strong base sites at T_{max} > 723 K in the CO_2-TPD profiles. $Rh/Ce_{0.8}Zr_{0.2}O_2$ possessed strong base sites on the surface like Rh/CeO_2 because the Zr^{4+} ions were introduced into the CeO_2 lattices in $Rh/Ce_{0.8}Zr_{0.2}O_2$. When x was larger than 0.2 in $Rh/Ce_{1-x}Zr_xO_2$, some Zr^{4+} ions could not enter in the CeO_2 lattices and they were distributed on the catalyst surface. The acidic Zr^{4+} ions on the surface decreased the base strength of catalysts [20–22].

Table 1 sums the TPD quantitative results of various catalysts. The desorption of water which formed from surface hydroxyls could be detected by Q-mass in every TPD measurement. Because the amount of water was almost the same (about 3–4 μmol/g) in each TPD measurement, the water desorption did not affect the results of NH_3-TPD and CO_2-TPD. The Rh/CeO_2 sample was calcined at 723 K and it could not adsorb NH_3 molecule on the surface in this study. Moreover, a Pd/CeO_2 sample which was calcined at 623 K also did not show a signal in the NH_3-TPD [32]. These results indicate that the CeO_2 support calcined at a low temperature (<723 K) does not possess appreciable surface acidity. On the other hand, it has been reported that a CeO_2 sample calcined at 1123 K showed a signal in the NH_3-TPD [33]. It seems that calcination at a high temperature of 1123 K could create some acid sites on the CeO_2 surface. From Table 1, the number of surface acidic sites increased

Table 1
TPD quantitative results of various catalysts.

Catalyst	CO_2 (TPD) (μmol/g)	NH_3 (TPD) (μmol/g)	H_2O (TPD) (μmol/g)
Rh/CeO_2	289	0	3
$Rh/Ce_{0.8}Zr_{0.2}O_2$	276	33	4
$Rh/Ce_{0.5}Zr_{0.5}O_2$	313	59	3
$Rh/Ce_{0.2}Zr_{0.8}O_2$	304	116	3
Rh/ZrO_2	241	228	4

Table 2
Weak, medium-strength, and strong CO_2-binding sites in various catalysts.

Catalyst	CO_2 (μmol/g)		
	Weak (T < 523 K)	Medium (523 < T < 723 K)	Strong (T > 723 K)
Rh/CeO_2	177	9	103
$Rh/Ce_{0.8}Zr_{0.2}O_2$	166	28	82
$Rh/Ce_{0.5}Zr_{0.5}O_2$	175	120	18
$Rh/Ce_{0.2}Zr_{0.8}O_2$	178	122	4
Rh/ZrO_2	176	65	0

with increasing Zr amount but the number of surface basic sites did not show a relation to the Zr amount in the $Rh/Ce_{1-x}Zr_xO_2$ samples.

Table 2 lists the weak, medium-strength, and strong CO_2-binding sites in various catalysts. The adsorbed CO_2 molecules desorbed from weak basic sites at low temperatures and desorbed from strong basic sites at high temperatures. As shown in Table 2, the amount of weak basic sites was almost invariable when Zr amount was changed in the $Rh/Ce_{1-x}Zr_xO_2$ samples. On the other hand, the amount of strong basic decreased with increasing Zr amount in the $Rh/Ce_{1-x}Zr_xO_2$ samples. Introducing Zr in Rh/CeO_2 decreased the amount of strong basic sites and introducing Ce in Rh/ZrO_2 increased the amount of strong basic sites. As a result, the basic amount could not be controlled but the basic strength could be designed through changing x value in the $Rh/Ce_{1-x}Zr_xO_2$ catalysts.

3.2. Catalytic synthesis of ethanol from syngas over Rh-based catalysts

Table 3 shows the reaction results of the synthesis of ethanol from syngas over various catalysts with 2 wt% Rh loading at 548 K. Rh/CeO_2 showed a CO conversion of 23.7%, which was much higher than those over Rh/SiO_2 (10.1%), Rh/MgO (10.8%), and Rh/ZrO_2 (18.2%). CeO_2-supported metal catalysts possess a strong interaction between support and metal (SISM) and thus they showed high catalytic performance for some reactions [16–18,34,35]. The SISM effect is important for improving catalytic activity in the synthesis of ethanol from syngas over Rh-supported catalysts [10,12,36,37]. The SISM effect contains several factors and the reducibility of support is an important factor for the Rh-based catalysts [10]. We think that the reducibility of CeO_2 support gave Rh/CeO_2 a higher CO conversion in the synthesis of ethanol. It has been reported that (Rh_x^0–Rh_y^+)–O–M is the active site for the formation of C_2-oxygenates [38]. Thus both Rh^0 species and Rh^+ species are important for the synthesis of ethanol from syngas [38]. Because a redox equilibrium ($Ce^{4+} + Rh^0 \leftrightarrow Ce^{3+} + Rh^+$) exists between CeO_2 support and Rh particles, both Rh^0 species and Rh^+ species can be stabilized in Rh/CeO_2. Moreover, the use of multicomponent precursors may yield well-dispersed metal particles on the surface of supports after calcination and reduction; this property, known as solid-phase crystallization (SPC), is important in the preparation of highly active metal-supported catalysts [16–18,39,40]. In Rh/CeO_2 catalyst, Rh^{3+} might enter in the Ce^{4+} position after calcination, and then highly dispersed Rh particles could be formed during the catalyst pretreatment (H_2 reduction) [9,18]. These Rh particles have uniformed small size and strong interaction with CeO_2 support, which also contributed to the high conversion over Rh/CeO_2.

As shown in Table 3, $Rh/Ce_{0.8}Zr_{0.2}O_2$ showed a higher conversion (27.3%) than that over Rh/CeO_2 (23.7%) and Rh/ZrO_2 (18.2%). Because $Ce_{0.2}Zr_{0.8}O_2$ support is a CeO_2-structured solid solution with the largest amount of Zr^{4+} ions, $Rh/Ce_{0.8}Zr_{0.2}O_2$ possesses a higher BET surface area and a smaller Rh particle size than those of Rh/CeO_2 and Rh/ZrO_2 (Fig. 2). The physical improvement (Rh particle and BET surface area) is one reason for the high CO conversion in the synthesis of ethanol over $Rh/Ce_{0.8}Zr_{0.2}O_2$. On the other hand,

Table 3
Reaction results of the synthesis of ethanol from syngas over various catalysts with 2 wt% Rh loading at 548 K.[a]

Catalyst	Conv./%	Oxygenate selectivity/%						HC select./%		CO_2 select./%
		MeOH	EtOH	$C_{3+}OH$	CH_3CHO	AcOEt	Other[b]	CH_4	C_{2+}	
Rh/SiO_2	10.1	3.3	16.2	1.1	13.3	4.6	3.9	42.9	12.5	2.2
Rh/ZrO_2	18.2	1.9	15.7	3.3	6.3	6.6	6.7	48.2	9.8	2.5
Rh/MgO	10.8	34.7	20.1	1.5	1.7	0.5	1.8	36.1	1.3	1.9
Rh/CeO_2	23.7	15.3	25.4	4.6	0.7	0.6	2.2	34.2	1.7	15.
$Rh/Ce_{0.8}Zr_{0.2}O_2$	27.3	7.9	35.2	4.9	1.4	0.8	1.9	35.7	2.1	10.1

[a] $P = 2.4$ MPa; $W/F = 10$ g h mol^{-1}; CO: 30%; H_2: 60%; N_2: 10%.
[b] Other oxygenates: CH_3COOCH_3, $HCOOCH_3$, $HCOOC_2H_5$, CH_3OCH_3, $CH_3OC_2H_5$; $C_2H_5OC_2H_5$, and CH_3COOH.

the introduction of Zr^{4+} ions into Rh/CeO_2 improved the reductibility of CeO_2 support (Fig. 3). The Rh^+ active species became more stable in the $Rh/Ce_{0.8}Zr_{0.2}O_2$ catalyst due to the high reductibility of $Ce_{0.8}Zr_{0.2}O_2$ support, which caused an increase of the SISM effect in the catalysts [9,18,41]. Thus the chemical improvement (reductibility) is another reason for the high CO conversion in the synthesis of ethanol over $Rh/Ce_{0.8}Zr_{0.2}O_2$.

As shown in Table 3, Rh/SiO_2 formed ethanol, acetaldehyde, and acetic acid ethyl ester (AcOEt) as main oxygenated products and the selectivity to methanol was low. Rh/ZrO_2 also formed the mixture of C_2-oxygenates as main oxygenated products although the selectivities for esters and ethers over Rh/ZrO_2 were higher than those over Rh/SiO_2 due to the acidity of ZrO_2 support. In contrast, basic supports MgO and CeO_2 supported Rh catalysts formed mixed alcohols (CH_3OH, C_2H_5OH, and $C_{3+}OH$) as main oxygenated products and the selectivities for acetaldehyde and AcOEt were low. Therefore, the Rh particles supported on neutral or acidic supports formed the mixture of C_2-oxygenates and the Rh particles supported on basic supports formed mixed alcohols from syngas. Hydrocarbons were formed over each Rh-based catalyst and the amount was in an order of $Rh/ZrO_2 > Rh/SiO_2 > Rh/MgO > Rh/CeO_2$. The Rh particles supported basic supports formed a small amount of hydrocarbons in the synthesis of ethanol from syngas.

Fig. 6 shows the reaction route for the formation of C_2 oxygenates from syngas over Rh-based catalysts. During the reaction, CO and H_2 molecules were adsorbed on Rh sites to form CO_{ad} and H_{ad} species, and then one CO_{ad} reacted with two H_{ad} to form a $CHOH_{ad}$ intermediate on the catalyst surface [42]. The $CHOH_{ad}$ intermediate could form a CH_3OH molecule by hydrogenation or form a $(CH_2)_{ad}$ intermediate by hydrogenation and dehydration [42]. Further, the $(CH_2)_{ad}$ intermediates could form CH_4 by hydrogenation or form C_2-oxygenated compounds by CO insertion [42–44]. The acidic supports promoted the dehydration process of forming $(CH_2)_{ad}$ intermediates from $CHOH_{ad}$ intermediates, which increased the concentration of $(CH_2)_{ad}$ intermediates in the catalytic system, and thus increased the selectivities for C_2-oxygenated compounds and CH_4. In contrast, the basic supports inhibited the dehydration process from $CHOH_{ad}$ intermediates to $(CH_2)_{ad}$ intermediates, which increased the concentration of $CHOH_{ad}$ intermediates in the catalytic system, and thus increased the selectivity for methanol.

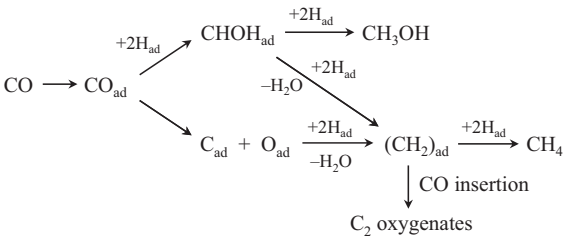

Fig. 6. Reaction route for the formation of C_2 oxygenates from syngas over Rh-based catalysts.

Rh/CeO_2 showed a higher selectivity for ethanol (25.4%) than that over Rh/MgO (20.1%) at 548 K although both CeO_2 and MgO are basic supports (Table 1). Rh^+ species is stable in Rh/CeO_2 ($Ce^{4+} + Rh^0 \leftrightarrow Ce^{3+} + Rh^+$) but it is difficult to be formed in Rh/MgO during the reaction. Rh^+ species is more active as comparison to the reduced Rh^0 species for CO insertion, and the insertion of CO to $(CH_2)_{ad}$ intermediates is the key step for producing C_{2+} oxygenates from syngas [12,31,37–39]. Therefore, Rh/CeO_2 showed a much higher ratio of ethanol to methanol (1.66) than that over Rh/MgO (0.58) at 548 K. On the other hand, the selectivity for CO_2 over Rh/CeO_2 (15.3%) was much higher than that over Rh/MgO (1.9%). The oxygen species moved from bulk to surface and oxidized CO to CO_2 over Rh/CeO_2 due to the oxygen mobility and oxygen storage capacity of CeO_2 support [27,28].

As shown in Table 3, $Rh/Ce_{0.8}Zr_{0.2}O_2$ formed mixed alcohols as main oxygenated products like Rh/CeO_2 because $Rh/Ce_{0.8}Zr_{0.2}O_2$ had strong base sites on the surface like Rh/CeO_2 (Fig. 5). However, the selectivity for ethanol over $Rh/Ce_{0.8}Zr_{0.2}O_2$ (35.2%) was higher than that over Rh/CeO_2 (25.4%). We think that two factors improved the selectivity for ethanol over $Rh/Ce_{0.8}Zr_{0.2}O_2$. Firstly, $Rh/Ce_{0.8}Zr_{0.2}O_2$ had acid sites by introducing Zr ions into the CeO_2 lattices (Fig. 4). The acid sites could promote the dehydration process of $CHOH_{ad}$ intermediates and increase the concentration of $(CH_2)_{ad}$ intermediates in the catalytic system. Because $CHOH_{ad}$ is a precursor of methanol and $(CH_2)_{ad}$ is a precursor of C_2-oxygenates (by CO insertion), $Rh/Ce_{0.8}Zr_{0.2}O_2$ showed a higher selectivity for ethanol than that over Rh/CeO_2. Secondly, $Rh/Ce_{0.8}Zr_{0.2}O_2$ possesses a larger amount of Rh^+ species on the surface because the reductibility of $Rh/Ce_{0.8}Zr_{0.2}O_2$ increased by introducing Zr^{4+} ions into CeO_2 lattices (Fig. 3). Rh^+ species promoted the insertion of CO to $(CH_2)_{ad}$ intermediates and improved the selectivity for ethanol over $Rh/Ce_{0.8}Zr_{0.2}O_2$.

Fig. 7 shows the effect of x in $Rh/Ce_{1-x}Zr_xO_2$ with 2 wt% Rh loading for the synthesis of ethanol at 548 K. Both the CO conversion and the selectivity for ethanol showed the maximum values at $x = 0.2$ in $Rh/Ce_{1-x}Zr_xO_2$. Because small-sized Zr^{4+} ions can be introduced into the Ce^{4+} positions till $x = 0.2$ in $Rh/Ce_{1-x}Zr_xO_2$, $Ce_{0.8}Zr_{0.2}O_2$ is a solid solution but $Ce_{0.7}Zr_{0.3}O_2$ and $Ce_{0.5}Zr_{0.5}O_2$ are not solid solutions [9,18]. The exceed Zr^{4+} ions in $Ce_{0.7}Zr_{0.3}O_2$ and $Ce_{0.5}Zr_{0.5}O_2$ formed ZrO_2 particles on the catalyst surface, which caused a decrease of the CO conversion in the synthesis of ethanol. Moreover, the acidic ZrO_2 particles on the catalyst surface at $x > 0.2$ in $Rh/Ce_{1-x}Zr_xO_2$ greatly increased the amounts of hydrocarbons and acetaldehyde in the products and decreased the selectivity for ethanol. On the other hand, the selectivity for methanol was high when x was less than 0.2 in $Rh/Ce_{1-x}Zr_xO_2$ due to the lack of acid sites. Therefore, acid sites are important to form C_{2+} oxygenates from syngas but excess acid sites decrease the selectivity for ethanol due to the formation of hydrocarbons and acetaldehyde. $Rh/Ce_{0.8}Zr_{0.2}O_2$ showed the highest catalytic performance among various $Rh/Ce_{1-x}Zr_xO_2$ catalysts for the synthesis of ethanol from syngas owing to strong reducibility and properly acidic–basic ability.

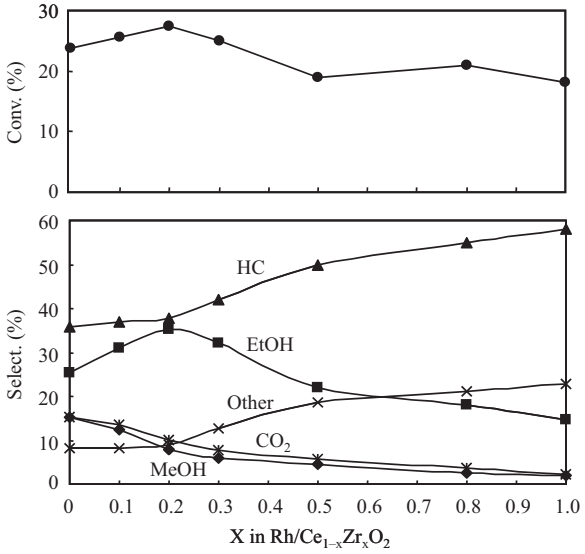

Fig. 7. Effect of x in $Rh/Ce_{1-x}Zr_xO_2$ with 2 wt% Rh loading for the synthesis of ethanol at 548 K. (●) CO conversion; (▲) selectivity to hydrocarbons; (■) selectivity to ethanol; (♦) selectivity to methanol; (×) selectivity to other oxygenates; (*) selectivity to CO_2. P = 2.4 MPa; W/F = 10 g h mol^{-1}; CO: 30%; H_2: 60%; N_2: 10%.

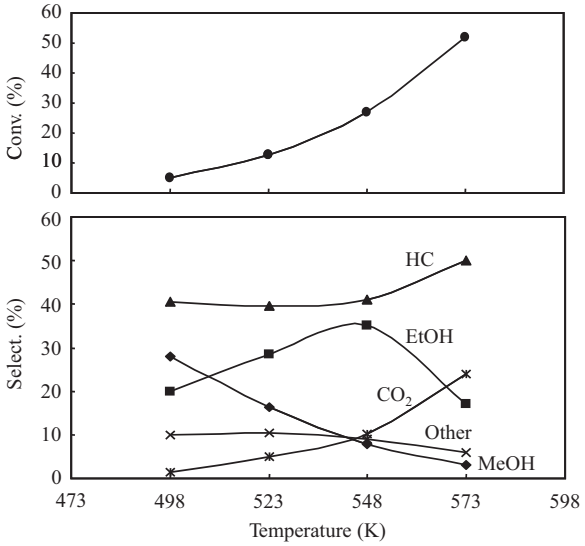

Fig. 9. Effect of reaction temperature in the synthesis of ethanol from syngas over $Rh/Ce_{0.8}Zr_{0.2}O_2$ with 2 wt% Rh loading. (●) CO conversion; (▲) selectivity to hydrocarbons; (■) selectivity to ethanol; (♦) selectivity to methanol; (×) selectivity to other oxygenates; (*) selectivity to CO_2. P = 2.4 MPa; W/F = 10 g h mol^{-1}; CO: 30%; H_2: 60%; N_2: 10%.

Fig. 8 shows the dependence of contact time in the synthesis of ethanol from syngas over $Rh/Ce_{0.8}Zr_{0.2}O_2$ with 2 wt% Rh loading at 548 K. The CO conversion increased from 8.4 to 39.2% when the W/F value increased to from 2.5 to 20 g h mol^{-1}, but a linear relation was only obtained when the W/F value was smaller than 10 g h mol^{-1}. The selectivities for hydrocarbons and other oxygenates were kept at almost the same values under various W/F values for the synthesis of ethanol from syngas. The selectivity for ethanol increased and the selectivity for methanol decreased with increasing W/F value over $Rh/Ce_{0.8}Zr_{0.2}O_2$. These results indicated that a high W/F value was favorable to increase to the yield of ethanol in the synthesis of ethanol from syngas over $Rh/Ce_{0.8}Zr_{0.2}O_2$.

Fig. 9 shows the effect of reaction temperature in the synthesis of ethanol from syngas over $Rh/Ce_{0.8}Zr_{0.2}O_2$ with 2 wt% Rh loading.

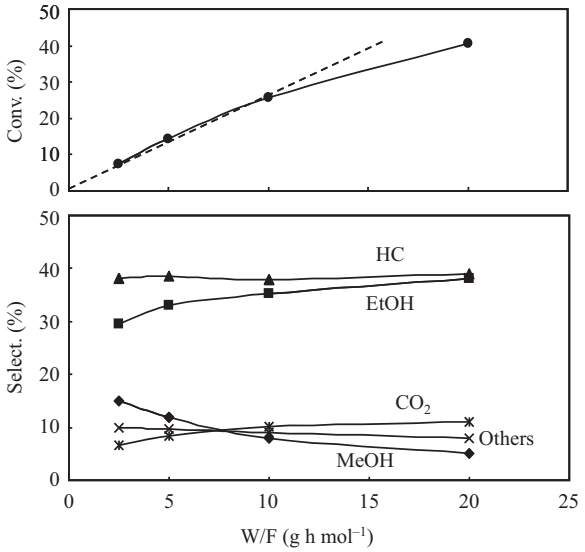

Fig. 8. Dependence of contact time in the synthesis of ethanol from syngas over $Rh/Ce_{0.8}Zr_{0.2}O_2$ with 2 wt% Rh loading at 548 K. (●) CO conversion; (▲) selectivity to hydrocarbons; (■) selectivity to ethanol; (♦) selectivity to methanol; (×) selectivity to other oxygenates; (*) selectivity to CO_2. Catalyst amount: 1 g; P = 2.4 MPa; feed gas: CO: 30%; H_2: 60%; N_2: 10%.

The CO conversion increased from 4.1 to 53.7% when the reaction temperature was increased from 498 to 573 K over $Rh/Ce_{0.8}Zr_{0.2}O_2$. The selectivity for methanol decreased and the selectivity for CO_2 increased with increasing reaction temperature for the synthesis of ethanol from syngas. The selectivity for methane was kept at almost the same values from 498 to 548 K but increased when the reaction temperature was higher than 548 K. As for the selectivity for ethanol, it increased with increasing reaction temperature from 498 to 548 K but decreased when the reaction temperature was higher than 548 K. These results indicated that 548 K was a suitable reaction temperature for the synthesis of ethanol from syngas over $Rh/Ce_{0.8}Zr_{0.2}O_2$.

4. Conclusions

The reducibility, acidity, and basicity of supports greatly influenced the catalytic activity and the product distribution for the synthesis of ethanol from syngas over Rh-based catalysts. Rh particles supported on neutral or acidic supports formed the mixture of C_2-oxygenates as main oxygenated products, and Rh particles supported on basic supports formed mixed alcohols as main oxygenated products. Acid sites were important to form C_{2+} oxygenates from syngas but excess acid sites decreased the selectivity for ethanol due to the formation of hydrocarbons and acetaldehyde. Zr^{4+} ions could be introduced into the CeO_2 lattices to form a solid solution when x was less than 0.2 in $Rh/Ce_{1-x}Zr_xO_2$. $Rh/Ce_{0.8}Zr_{0.2}O_2$ showed the highest CO conversion and the highest selectivity for ethanol among various $Rh/Ce_{1-x}Zr_xO_2$ catalysts because the introduction of Zr^{4+} ions into CeO_2 lattices increased the reducibility of support and brought weak acid sites to the basic CeO_2 support. A high W/F value was favorable to increase the yield of ethanol over $Rh/Ce_{0.8}Zr_{0.2}O_2$. The selectivity for ethanol increased with increasing reaction temperature from 498 to 548 K but decreased when the temperature was higher than 548 K over $Rh/Ce_{0.8}Zr_{0.2}O_2$.

References

[1] J.J. Spivey, A. Egbebi, Chem. Soc. Rev. 36 (2007) 1514.
[2] V. Subramani, S.K. Gangwal, Energy Fuel 22 (2008) 814.
[3] R. Burch, M.J. Hayes, J. Catal. 165 (1997) 249.
[4] M.A. Haider, M.R. Gogate, R.J. Davis, J. Catal. 261 (2009) 9.

[5] J. Hu, Y. Wang, C. Cao, D.C. Elliott, D.J. Stevens, J.F. White, Catal. Today 120 (2007) 90.
[6] J. Bao, Z. Sun, Y. Fu, G. Bian, Y. Zhang, N. Tsubaki, Top. Catal. 52 (2009) 789.
[7] X. Dong, X. Liang, H. Li, G. Lin, P. Zhang, H. Zhang, Catal. Today 147 (2009) 158.
[8] X. Sun, G.W. Robert, Appl. Catal. A: Gen. 247 (2003) 133.
[9] Y. Liu, K. Murata, M. Inaba, I. Takahara, K. Okabe, J. Jpn. Petrol. Inst. 53 (2010) 153.
[10] R. Burch, M.I. Petch, Appl. Catal. A: Gen. 88 (1992) 39.
[11] H. Luo, W. Zhang, H. Zhou, S. Huang, P. Lin, Y. Ding, L. Lin, Appl. Catal. A: Gen. 214 (2001) 161.
[12] Y. Du, D. Chen, K. Tsai, Appl. Catal. A: Gen. 35 (1987) 77.
[13] A. Kiennemann, R. Breault, J.P. Hindermann, J. Chem. Soc. Faraday Trans. I 83 (1987) 2119.
[14] N. Tsubaki, K. Fujimoto, Top. Catal. 22 (2003) 325.
[15] Y. Liu, T. Hayakawa, K. Suzuki, S. Hamakawa, T. Tsunoda, T. Ishii, M. Kumagai, Appl. Catal. A: Gen. 223 (2002) 137.
[16] Y. Liu, T. Hayakawa, T. Tsunoda, K. Suzuki, S. Hamakawa, K. Murata, R. Shiozaki, T. Ishii, M. Kumagai, Top. Catal. 22 (2003) 205.
[17] Y. Liu, T. Hayakawa, K. Suzuki, S. Hamakawa, Catal. Commun. 2 (2001) 195.
[18] Y. Liu, T. Hayakawa, T. Ishii, M. Kumagai, H. Yasuda, K. Suzuki, S. Hamakawa, K. Murata, Appl. Catal. A: Gen. 210 (2001) 301.
[19] W. Khaodee, B. Jongsomjit, S. Assabumrunbrat, P. Praserthdam, S. Goto, Catal. Commun. 8 (2007) 548.
[20] E.I. Gurbus, E.L. Kunkes, J.A. Dumesic, Appl. Catal. B: Environ. 94 (2010) 134.
[21] E.I. Gurbus, E.L. Kunkes, J.A. Dumesic, J. Catal. 266 (2009) 236.
[22] S.C. Dantas, J.C. Escritori, R.R. Soares, C.E. Hori, Chem. Eng. J. 156 (2010) 380.
[23] J.A. Dean (Ed.), Lang's Handbook of Chemistry, 23th ed., McGraw-Hill, New York, 1985.
[24] P. Gronchi, E. Tempesti, C. Mazzocchia, Appl. Catal. A: Gen. 120 (1994) 115.
[25] J.A. Wang, T. Lopez, X. Bokhimi, O. Novaro, J. Mol. Catal. A: Chem. 239 (2005) 249.
[26] E. Rocchini, M. Vicario, J. Llorca, C. Leitenburg, G. Dolcetti, A. Trovarelli, J. Catal. 211 (2002) 407.
[27] D. Terribile, A. Trovarelli, C. Leitenburg, A. Primavera, G. Dolcetti, Catal. Today 47 (1999) 133.
[28] C. Leitenburg, A. Trovarelli, J. Llorca, F. Cavani, G. Bini, Appl. Catal. A: Gen. 139 (1996) 161.
[29] S. Imamura, T. Higashihara, Y. Saito, H. Aritani, H. Kanai, Y. Matsumura, N. Tsuda, Catal. Today 50 (1999) 369.
[30] P. Fornasiero, J. Kaspar, V. Sergo, M. Graziani, J. Catal. 182 (1999) 56.
[31] C. Diagne, H. Idriss, A. Kiennemann, Catal. Commun. 3 (2002) 565.
[32] E.I. Gurbuz, E.L. Kunkes, J.A. Dumesic, Appl. Catal. B: Environ. 94 (2010) 134.
[33] J. Miao, L. Yang, J. Cai, Surf. Interface Anal. 28 (1999) 123.
[34] W. Shen, Y. Ichihashi, Y. Matsumura, Catal. Lett. 79 (2002) 125.
[35] H. Roh, Y. Wang, D. King, Top. Catal. 49 (2008) 32.
[36] H. Orita, S. Naito, K. Tamaru, J. Chem. Soc., Chem. Commun. (1983) 993.
[37] P. Meriaudeau, H. Ellestad, C. Naccache, J. Mol. Catal. 17 (1982) 219.
[38] Y. Wang, H. Luo, D. Liang, X. Bao, J. Catal. 196 (2000) 46.
[39] Y. Liu, K. Murata, M. Inaba, N. Mimura, Appl. Catal. A: Gen. 309 (2006) 91.
[40] Y. Liu, K. Murata, T. Hanaoka, M. Inaba, K. Sakanishi, J. Catal. 248 (2007) 277.
[41] H.S. Roh, Y. Wang, D.L. King, Top. Catal. 49 (2008) 32.
[42] A. Takeuchi, J.R. Katzer, J. Phys. Chem. 86 (1982) 2438.
[43] S.S.C. Chuang, R.W. Stevens Jr., R. Khatri, Top. Catal. 32 (2005) 225.
[44] M. Bowker, Catal. Today 15 (1992) 77.